arXiv:astro-ph/9706270v1 26 Jun 1997

Dwarf galaxies in four rich clusters with $0.02 < z < 0.14$

Neil Trentham

Institute for Astronomy, University of Hawaii

2680 Woodlawn Drive, Honolulu HI 96822, U. S. A.

email : nat@newton.ifa.hawaii.edu

Submitted to *MNRAS*

ABSTRACT

Deep measurements are presented of four rich clusters of galaxies: Abell 1367 ($z = 0.022$), Abell 2199 ($z = 0.030$), Abell 1795 ($z = 0.063$), and Abell 1146 ($z = 0.141$). All clusters have an excess of galaxies at faint magnitudes above blank sky fields. We correct for background contamination and measure the luminosity function of these galaxies in each cluster, and then combine these luminosity functions to get better statistics. The resultant combined luminosity function is rising at faint magnitudes, with a logarithmic slope $-1.5 < \alpha < -1.2$ for $-18 < M_B < -13$ and $-19 < M_R < -15$. This is similar to what has been observed independently in the Coma cluster. The colours of these faint galaxies suggest that they are dwarf spheroidals.

Key words: galaxies: clusters: luminosity function – galaxies: clusters: individual: A1367, A2199, A1795, A1146

1 INTRODUCTION

Galaxies have masses which vary by at least six orders of magnitude. Yet they separate unambiguously into just two distinct classes of objects in the fundamental plane parameter correlations (see e.g. Kormendy 1985, 1987; Binggeli 1994). The first of these is the early-type giants and bulges of disk galaxies, which have increasing surface-brightness as their total luminosity increases. The second of these are the late-type giant and dwarf galaxies which have decreasing surface-brightness as their total luminosity increases (they also have increasing dark matter fractions as their total luminosity decreases; Kormendy 1990). The giant galaxies have been well studied over the last fifty years, but the properties of the dwarf galaxies population are only now beginning to be described in detail.

The first such measurements were of the Local Group dwarfs (see Hodge 1989 for a review) and of the dwarfs in nearby poor groups (Ferguson & Sandage 1991) and poor clusters like Virgo (Sandage et al. 1985) and Fornax (Ferguson 1989). These measurements showed that dwarf galaxies have a luminosity function (LF: $\phi(L) \propto L^{\alpha}$) that is rising as $\alpha = -1.35$ at the faintest magnitudes probed ($M_B \sim -13$ for $H_0 = 75$ km s^{-1} Mpc^{-1}). In these poor clusters and groups, overwhelmingly the most numerous galaxy type at faint magnitudes ($M_B < -16$) are the dwarf spheroidal (dSph), alternatively called dwarf elliptical, galaxies (see Binggeli 1987, 1994; Ferguson & Binggeli 1994). These galaxies have similar scaling laws to dwarf irregulars (dIrr) in the fundamental plane correlations, but are redder, because old stellar populations contribute proportionately more of the light.

Another important development has been the detection of a population of low-luminosity star-forming galaxies in the field at $z > 0.2$ (Broadhurst et al. 1988, Cowie et al. 1991). These contribute a significant, but probably not the dominant (see Cowie et al. 1995, 1996), contribution to the excess blue counts observed there. The fate of these galaxies is not known, but they might evolve into low surface-brightness galaxies (McGaugh 1994, Ferguson & McGaugh 1995), perhaps similar to the dwarf spheroidal galaxies observed today (Kormendy & Bender 1994).

More recently, measurements of dwarf galaxies in rich clusters have been made. This is now technically feasible because the contamination from background galaxies at faint magnitudes has been quantified well (Driver et al. 1994, Bernstein et al. 1995, Trentham 1997a) and can be corrected for, allowing LFs to be computed. Previous studies of clusters concentrated on giant galaxies; these bright galaxies are sufficiently numerous relative to the background that contamination effects are small. Much of the recent work has concentrated on clusters at $z \sim 0.2$ like Abell 963 (Driver et al. 1994, Trentham 1997b), Abell 665 (Wilson et al. 1997, Trentham 1997b), and Abell 1689 (Wilson et al. 1997). This redshift is particularly interesting because it is where the low-luminosity star-forming galaxies that contribute to the excess blue counts begin to appear. However, in clusters this distant, measurements of dwarf galaxies that are in the cluster can only be made down to $M_B \sim -15$, so that they probe only a small part of the magnitude range where the dwarfs dominate. Nevertheless, it is interesting to note that the dwarfs seen in these clusters appear to be red (Trentham 1997b). Fainter dwarfs have been observed in the Coma cluster at $z = 0.023$ (Secker & Harris 1996, Trentham 1997c) and are very numerous there, with $-1.4 < \alpha < -1.7$ fainter than $M_R = -16$. These dwarf galaxies have $1.3 < B - R < 1.5$, and are probably dSphs.

In this work, we present similar measurements for four more clusters, with $0.022 < z < 0.14$. This will permit us to see if the results found in Coma are a universal feature of rich clusters (Coma is anomalous in its X-ray properties as it has no cooling flow − Hughes et al. 1988 − so that galaxy evolution might well proceed differently there to in other rich clusters), and if the LF or the colours of the dwarf galaxies in clusters vary with redshift.

Our sample is presented in Table 1. There we list the Abell (1958) richness, redshift z, velocity dispersion σ, X-ray luminosity L_x, Galactic extinction A_B along our line of sight, critical surface density for gravitational lensing of distant background galaxies Σ_c, and mass deposition rate $\dot{M}$ for the cooling flow clusters. Abell 1367 is at approximately the same distance as Coma, but is not as rich, and has lower X-ray luminosity (like Coma, it has no cooling flow). Its giant galaxy luminosity function has been measured by Godwin & Peach (1982) using photographic photometry. It is the next best example after Coma of a rich cluster at $z \sim 0.02$ with a galaxy density high enough that we might measure the dwarf galaxy LF. Abell 2199 and Abell 1795 are more distant. Both are rich cooling flow clusters with supergiant cD galaxies at their center. Abell 1795 has an anomalously low total giant galaxy optical luminosity given its X-ray gas mass (Arnaud et al. 1992); the measurements here will enable us to tell if some of this deficiency can be made up by an excess of dwarf galaxies. Abell 1146 is more distant, but is extremely rich; it is one of only seven richness 4 clusters in the Abell catalog and is significantly the nearest of these. Therefore it is a good candidate for having a detectable dwarf galaxy population.

Throughout this work we assume $H_0 = 75$ km s^{-1} Mpc^{-1} and $\Omega_0 = 1$.

2 OBSERVATIONS AND PHOTOMETRY

2.1 Observations and data preprocessing

In Figure 1, we present our images. The observing log is presented in Table 2, where we list the field position and size, total exposure time, average extinction $< X >$ due to clouds, and seeing, for each image. All observations were taken at the f/10 Cassegrain focus of the University of Hawaii 2.2 m telescope on Mauna Kea using a thinned Tektronix 2048 × 2048 CCD (scale $0\farcs22$ pixel^{-1}; field of view $7\farcm5 \times 7\farcm5$). Each image was constructed from a number of shorter exposures, of length $5 - 10$ minutes, dithered in order to reject cosmic rays and bad pixels. These images were bias-subtracted (the CCD dark current was negligible) and then flatfielded (the flatfield we used was constructed using both median sky and twilight flats) before being combined. The reduced images are flat to better than one percent.

Instrumental magnitudes were computed from observations of several (typically ~ 30 per night) standard stars and the photometry was converted to the Johnson (UBV) − Cousins (RI) magnitude system of Landolt (1992). This conversion is accurate to about 2%. Conditions were photometric when most of the images were taken; in the instances when there was thin cirrus overhead, the images were calibrated using shorter exposures taken under photometric conditions. Table 2 shows how big these corrections were.

2.2 Photometry techniques

We obtain total magnitudes for the galaxies we detect in our images by measuring isophotal magnitudes and making a correction that takes the surface-brightness of the galaxies into account. This method is described in detail elsewhere (Trentham 1997a); here we list the main steps in outline form and add comments that are specific to the data presented in this paper.

1) We measure the rms sky noise σ_{rms} and the FWHM seeing $b_{\rm FWHM}$ for each image. The sky Poisson noise is always the dominant noise source.

2) We then simulate galaxies of various apparent magnitudes and exponential scale-lengths. These simulated galaxies are then convolved with a Gaussian seeing function of width $b_{\rm FWHM}$ and Poisson noise of rms magnitude σ_{rms} is added.

3) We then run the FOCAS detection algorithm (Jarvis & Tyson 1981, Valdes 1982, 1989) on this image to search for objects with fluxes that are $3\sigma_{\rm rms}$ above the sky. For each object we measure the isophotal magnitude m_I and first-moment light radius r_1. As the true magnitude m of each object is known, we compute the function $m(m_I, r_1)$, and its uncertainty $\sigma(m)[m_I, r_1]$. The uncertainty comes from studying how intrinsically identical galaxies are detected differently depending on where they are placed in the image i.e. depending on the local noise. We also determine the faintest magnitude m_L at which galaxies whose intrinsic magnitudes and scale-lengths are equal to those of local dwarf galaxies projected to the distance of the cluster are detected with 100% completeness. This will be the faintest magnitude to which we determine the LF in each image. We make this cut because the completeness is a strong function of the detailed galaxy properties fainter than m_L, so trying to correct for this effect in our data is dangerous.

4) We then run the same detection algorithm on our data, and make a catalog of all objects detected at the 3σ level. For each object, we measure m_I and r_1. We also compute the aperture magnitude m_a within an aperture diameter of $3\farcs0$. These magnitudes will be used to measure colours. Isophotal magnitudes are not used for computing colours because the detection isophotes are not the same in the different bands. A $3\farcs0$ aperture is large enough that differential seeing effects between our B and R images are negligible.

5) Multiple objects within a single detection isophote are identified by searching for multiple maxima and are split into individual objects using the FOCAS splitting algorithm. The algorithm is run several times so that cases where many objects were contained in a single isophote initially are all individually recovered. The quantities m_I and r_1 are computed for each object at each stage of the splitting.

6) Objects are then classified (see Valdes 1989 for the details of the classification terminology) based on their morphology relative to that of several reference PSF stars in the field.

7) We then remove from the catalog: (i) objects whose $m(m_I, r_1) > m_L$; (ii) diffraction spikes of bright stars, ghost images, and chip defects (these were identified from the FOCAS classification – see Trentham 1997a and Valdes 1989 for details); (iii) spurious objects that were detected in the halos of bright stars and galaxies where the noise is much higher than in the rest of the image. The last of these corrections required us to look at all objects in our image that were part of a larger object that was subsequently split into more than three smaller objects in our original detection pass and make a judgment by eye as to whether the faint objects we see are real objects or enhanced noise peaks. Also, at this stage, a number of low surface brightness galaxies that had been recognized as a multiple object and split into many small objects centred on local noise peaks were reconstructed, and the values of m_I and r_1 computed prior to splitting were adopted.

8) After these corrections are made, we have a catalog of objects classified as “galaxies” or “stars”. At faint magnitudes, these classifications are unreliable because many galaxies have apparent scale lengths smaller than the seeing and so look like stars. We therefore correct

for stellar contamination at faint magnitudes by computing how many faint stars we expect given the number of bright ($m < 20$) stars and assuming that Galactic stellar luminosity function has the slope measured by Jones et al. 1991. The stellar contamination is small ($\sim 15\%$ at the faintest magnitudes in A1146, and much less in the other clusters) and the uncertainties generated by this method are also small.

9) For each object in our catalog we then use m_I and r_1 to compute m and its uncertainty $\sigma(m)$, correct for stellar contamination as in 8), and then bin the data in half-magnitude intervals. The number counts are then computed by dividing the number of galaxies in each bin by the survey area. This survey area includes a correction for crowding, the process by which faint galaxies go undetected because they happen to fall within the detection isophote of a much brighter object (see Trentham 1997a for details of how this was done).

10) The number counts were corrected for Galactic extinction using the HI maps of Burstein & Heiles (1982) and the colour conversions of Cardelli et al. (1989). Corrections to the background galaxies for gravitational lensing by the cluster dark matter (see Trentham 1997b) are $\sim 2\%$ for A1146 and much smaller for the other clusters. We neglect this effect, and also extinction from dust in the cluster (see Ferguson 1993, Bernstein et al. 1995).

As this stage, we have the number of galaxies per half-magnitude per square degree, as a function of apparent magnitude, for each of our cluster fields. The data are presented in Section 3.1, and we describe there how we compute the LF from them.

3 RESULTS AND DISCUSSION

3.1 Number Counts

The number count − magnitude relations computed as described in Section 2.2 are presented in Figure 2.

The uncertainties are the quadrature sum of counting statistics and uncertainties from the isophotal corrections $\sigma(m)$. The uncertainties from counting statistics dominate at the bright end, and the uncertainties from isophotal corrections dominate at the faint end. Also shown in Figure 2 are the mean background counts for random sky fields (Trentham 1997a). In each case, at progressively fainter magnitudes the background contributes more to the total number counts.

The luminosity function is computed by subtracting the background contribution from the number counts. The uncertainty is computed taking into account the field-to-field variance in the background in addition to the errors described in the last paragraph. This field-to-field variance in the background counts is discussed in detail in Trentham (1997a). We use the numbers there, corrected here for the differences in survey area using Poisson statistics.

In converting apparent magnitudes to absolute magnitudes, we assume distance moduli of 34.75 for A1367, 35.41 for A2199, 37.03 for A1795, and 38.83 for A1146.

3.2 Luminosity Functions

The LFs are presented in Figures 3 (B-band) and 4 (R-band). The uncertainties are the quadrature sum of errors from counting statistics, from uncertainties in the total magnitudes, and from the field-to-field variance in the background. The last of these dominates the error everywhere except at the brightest magnitudes, where counting statistics dominate.

The LF of Abell 1367 is very poorly constrained because of the large errors following background subtraction. This is because the galaxy density there is very low relative to the background. It is the poorest cluster studied here, but no richer clusters exist at $z \sim 0.02$ except Coma, which is studied elsewhere, and Perseus, which is close to the Galactic plane. Abell 2199 has a LF that is slowly rising towards fainter magnitudes ($\alpha \sim -1.4$) over the entire magnitude range. This rise is apparent in both the R-band and B-band data, but the R-band data has better statistics at the faint end ($M_R \sim -12$) following background subtraction. Also, the R-band data probe slightly deeper ($B - R \sim 1.3$ for faint galaxies; see Section 3.3). The extremely steep LF ($\alpha = -2.2$) claimed by De Propris et al.(1995) for the cD halo of NGC 6166 is not seen in our data. Their estimate of the field-to-field variance in the background (<1% probability of getting >1.4 times the mean counts in a

6.54 square arcminute field) is much smaller than our observed variance (16% of getting $>$1.4 times the mean counts in the same field at $B = 24$ and more than 16% at brighter magnitudes; see Trentham 1997a, also Driver et al. 1994, Bernstein et al. 1995). If our variance measurement is resonable, then the errors in each data point quoted by De Propris et al. must be underestimates. The uncertainty in their value of α then becomes large. This is the most natural explanation of the difference in their results and ours. Abell 1795 has a slightly flatter LF than Abell 2199, although we do not probe quite so faint. We do not see enough dwarf galaxies to explain away the decrement in optical luminosity relative to X-ray gas mass described in Section 1. Abell 1146 also has a shallow luminosity function for $-21 < M_R < -17$, but there is an intriguing sign of an upturn in the faintest point in both the R-band ($M_R = -16$) and B-band ($M_B = -15$) data.

All the LFs in each band were then combined to produce a composite LF, which we present in Figure 5 and Tables 3 and 4. This function falls seeply at bright magnitudes (the cluster cD galaxies push up the LF at the very bright end), and rises gradually towards faint magnitudes.

For comparison with previous deep work in other clusters and the field and with theory, it is useful to describe the LF at each magnitude by a slope parameter $\alpha(M) = -2.5\frac{\mathrm{d}\log_{10}N}{\mathrm{d}M} - 1$. One method that is frequently applied is to estimate $\alpha(M)$ using fitting functions like the Schechter (1976) function, in which $\alpha(M)$ tends to an asymptotic value α^* at faint magnitudes. Pitfalls of this approach are reviewed in Section 2 of Trentham (1997a). The major problems are (a) the fitting functions have no physical significance, and (b) they are susceptible to severe parameter coupling (e.g. the Schechter α^* and M^* are strongly coupled so that a value of α^* that we might derive is strongly affected by the properties of the bright galaxies which, as outlined in Section 1, are a separate population of stellar systems from the dwarf galaxies. In this work we use local linear and polynomial fits to estimate $\alpha(M)$ at each M. These fits do not have any physical significance either, but are more useful than Schechter fits for the present study because only galaxies with magnitudes close to M contribute in the derivation of $\alpha(M)$. We present in Tables 3 and 4 α_{mn}, where $-0.4(\alpha_{mn}+1)$ is the slope of $\log_{10} N$ at M of the best fitting polynomial of order m to the $2n+1$ points, computed at 1 magnitude intervals, centered on M. The case $m=1$ corresponds to a linear fit.

The tables show that $-1.5 < \alpha < -1.2$ for $-18 < M_B < -13$ and $-19 < M_R < -15$. This is similar to what has been observed in the Coma cluster in this magnitude range (Secker & Harris 1996, Trentham 1997c). The tables also show that $\alpha = -1$ is nowhere a good fit to the data: the LF is always rising. The LF is continuous over the magnitude range where there is a discontinuity between giants and dwarfs in the cluster fundamental plane (at $M_B \sim -16$). This is suggestive of a conspiracy in which the giant galaxy LF is falling by an amount almost exactly compensated for by the rise in the dwarf LF, on going to fainter magnitudes. Such an effect was also seen in the Virgo cluster (Sandage et al. 1985).

The pattern evident in Figure 5 is not visible in Figures 3 or 4 because the statistics in each cluster are poor; it is only when we combine all the data that the trend in Figure 5 becomes significant. The reason that the statistics in each cluster are poor is because the field-to-field variance in the background is high. In a separate paper (Trentham 1997d), we extend this analysis to a much larger sample of clusters from our own data, and from the literature. We obtain a much more tightly constrained LF and argue that the LF in clusters might be universal.

3.3 Colours

In Figure 6, we present the colours of galaxies having absolute magnitude $-16 < M_R < -15$ in the observed frame. This narrow magnitude range was chosen as it encompasses all magnitudes bright enough to be reliably probed by the data we have for all four clusters, while still being faint enough that the galaxies in this range are likely to be dwarf galaxies as defined by their fundamental plane positions (very few giant galaxies exist this faint; Binggeli 1987, 1994). The colours are computed as described in the figure caption and in Section 2.2 (step 4) of the text.

The colour distribution in Abell 1367 is essentially unconstrained, for the same reason that the LF is so poorly determined i.e. the galaxy density is too low relative to the background. The statistics for Abell 2199 and Abell 1795 are much better (although still not very good). The mean colour (corrected for background contamination) of galaxies blueward of giant ellipticals at the cluster redshift is $B - R = 1.31$ for Abell 2199 and $B - R = 1.70$ for Abell 1795. This colour cut removes galaxies which are very likely to be background galaxies (although they could, in principle, be reddened cluster members), and therefore improves the statistics. For Abell 1146, the mean colour of galaxies in excess of background with $1.0 < B - R < 2.8$ is $B - R = 2.06$ (here we impose a cut at the red end to remove background contamination, and at the blue end to assist in removing possible stellar contamination – see Figure 6). The mean colours, as computed above, are presented as a function of redshift in Figure 7. The figure suggests that in all cases here, and for Coma (where the statistics are much better), the galaxies are too red to be dwarf irregulars, and are probably dwarf spheroidals (see Trentham 1997b for a discussion of the colours of the different kinds of galaxies).

ACKNOWLEDGMENTS

This research has made use of the NASA/IPAC extragalactic database (NED) which is operated by the Jet Propulsion Laboratory, Caltech, under agreement with the National Aeronautics and Space Administration.

REFERENCES

Abell G. O., 1958, ApJS, 3, 211

Arnaud M., Rothenflug R., Boulade O., Vigroux L., Vangioni-Flam E., 1992, A&A, 254, 49

Bernstein G. M., Nichol R. C., Tyson J. A., Ulmer M. P., Wittman D., 1995, AJ, 110, 1507

Binggeli B., 1987, in Faber S. M., ed., Nearly Normal Galaxies. Springer-Verlag, New York, p. 195

Binggeli B., 1994, in Meylan G., Prugneil P., ed., ESO Conference and Workshop Proceedings No. 49: Dwarf Galaxies. European Space Observatory, Munich, p. 13

Broadhurst T. J., Ellis R. S., Shanks T., 1988, MNRAS, 235, 827

Burstein D., Heiles C., 1982, AJ, 87, 1165

Cardelli J. A., Clayton G. C., Mathis J. S., ApJ, 345, 245

Coleman G. D., Wu C-C., Weedman D. W., 1980, ApJS, 43, 393

Cowie L. L., Hu E. M., Songaila A., 1995, Nat, 377, 603

Cowie L. L., Songalia A., Hu E. M., 1991, Nat, 354, 460

Cowie L. L., Songaila A, Hu E. M., Cohen J. G., 1996, AJ, in press

De Propris R., Pritchet C. J., Harris W. E., McClure R. D., 1995, ApJ, 450, 534

Driver S. P., Phillipps S., Davies J. I., Morgan I., Disney M. J, 1994, MNRAS, 268, 393

Fabian A. C., 1994, ARAA, 32, 277

Ferguson H. C., 1989, AJ, 98, 367

Ferguson H. C., 1993, MNRAS, 263, 343

Ferguson H. C., Binggeli B., 1994, A&AR, 6, 67

Ferguson H. C, McGaugh S. S., 1995, ApJ, 440, 470

Ferguson H. C., Sandage A., 1991, AJ, 101, 765

Gioia I. M., Luppino G. A., 1994, ApJS, 94, 583

Girardi M., Fadda D., Giuricin G., Mardirossian F., Mezetti M., Biviano A., 1996, ApJ, 457, 61

Godwin J. G., Peach J. V., 1982, MNRAS, 200, 733

Hodge P. W., 1989, ARAA, 27, 139

Hughes J. P., Gorenstein F., Fabricant D., 1988, ApJ, 329, 82

Jarvis J. F., Tyson J. A., 1981, AJ, 86, 476

Jones C., Forman W., 1984, ApJ, 276, 38

Jones L. R., Fong R., Shanks T., Ellis R. S., Peterson B. A., 1991, MNRAS, 249, 481.

Kormendy J., 1985, ApJ, 295, 73

Kormendy J., 1987, in Faber S. M. ed., Nearly Normal Galaxies. Springer-Verlag, New York, p. 163

Kormendy J., 1990, in Kron R. G., ed., The Edwin Hubble Centennial Symposium: The Evolution of the Universe of Galaxies. Astronomical Society of the Pacific, San Francisco, p. 33

Kormendy J., Bender R., 1994, in Meylan G., Prugneil P., ed., ESO Conference and Workshop Proceedings No. 49: Dwarf Galaxies. European Space Observatory, Munich, p. 161

Landolt A. U., 1992, AJ, 104, 340

McGaugh S. S., 1994, Nature, 367, 538

Sandage A., Binggeli B., Tammann G. A., 1985, AJ, 90, 1759

Schechter P., 1976, ApJ, 203, 297

Secker J., 1996, preprint

Secker J., Harris W. E., 1996, ApJ, 469, 628

Trentham N., 1997a, MNRAS, in press

Trentham N., 1997b, MNRAS, submitted

Trentham N., 1997c, MNRAS, submitted

Trentham N., 1997d, MNRAS, submitted

Valdes F., 1982, Proc. SPIE, 331, 465

Valdes F., 1989, in Grosbol P. J., Murtagh F., Warmels R. H., ed., ESO Conference and Workshop Proceedings No. 31: Proceedings of the 1st ESO/St-ECF Data Analysis Workshop. European Space Observatory, Munich, p. 35

Wilson G., Smail I., Ellis R. S., Couch W. J., 1997, MNRAS, in press

Zabludoff A. I., Huchra J.P., Geller M. J., 1990, ApJS, 74, 1

FIGURE CAPTIONS

Figure 1. The R-band images of our fields. North is up and east is to the left in all images; the field sizes are given in Table 2. The cD galaxy (NGC 6166) of A2199 is to the west of Field II, and its outer halo is visible in part to the right of the image. The cD galaxies of A1795 and A1146 are the brightest galaxies in those images.

Figure 2. The number count $-$ magnitude relations, computed as described in the text. For A2199, the data from both fields are included. The dashed lines in each figure are the mean background counts from Trentham (1997a).

Figure 3. The B-band luminosity functions for the sample clusters. Slopes corresponding to $\alpha = -2$ and $\alpha = -1$ are shown in each panel.

Figure 4. The R-band luminosity functions for the sample clusters. Slopes corresponding to $\alpha = -2$ and $\alpha = -1$ are shown in each panel.

Figure 5. The composite luminosity function for the 4 clusters in this survey. Both the B-band (upper panel) and R-band (lower panel) functions are shown. These are the weighted average of the individual luminosity functions shown in Figures 3 and 4, where each cluster is normalized to have the same number of galaxies brighter than $M_B = -16.5$ or $M_R = -17.5$. The vertical scales are arbitrarily chosen to correspond to that of a cluster with 1000 galaxies deg^{-2} brighter than $M_B = -16.5$ or $M_R = -17.5$ (this would be a typical Abell richness 2 cluster). Slopes corresponding to $\alpha = -2$ and $\alpha = -1$ are shown in each panel.

Figure 6. Colour histograms for the sample clusters. Only galaxies whose isophotal magnitudes satisty the condition $-16 < R - \mu < -15$ are included in these plots, where R is the isophotal magnitude and μ is the distance modulus listed in Section 3.1 of the text. Only objects classified as “galaxy” in both B and R images are included, except for A1146, where we include all objects classified as “galaxy” in just the R-band image (the reddest objects appear very small and faint in the B-band image of A1146, and are subject to misclassification as “stars”). All colours are measured within a $3.''0$ diameter

aperture centered on the galaxy. The histograms include a background subtraction, using the background data presented in Trentham 1997a; the background measurements were made in an identical way to the cluster measurements in each case. In some cases there were more galaxies in the background field per square degree than galaxies in the cluster field in a given bin − hence the negative values on the ordinate axis.

Horizontal error bars are small. Vertical error bars correspond to the quadrature sum of the cluster field and background error bars. Typically, the background counts in each bin are of the same order of magnitude as the cluster counts, so that an estimate of the vertical error in each bin is $\sqrt{2N}$ where N is the number of galaxies. These are generally very large. The histograms are complete to at least $B - R \sim 2.7$ in all cases.

Figure 7. The mean colour of the excess galaxies detected above the background with $-16 < R - \mu < -15$, as a function of the cluster redshift. These numbers are computed as described in the text. The Coma point is from Secker (1996). Predicted curves for dIrr and giant ellipticals are presented; these use the K-corrections of Coleman et al. (1980). The shaded region is where we predict local dSphs to lie, given the K-corrections of Trentham (1997b). The dSphs exhibit a range in colour, because they exhibit a range in metallicity and star formation history.

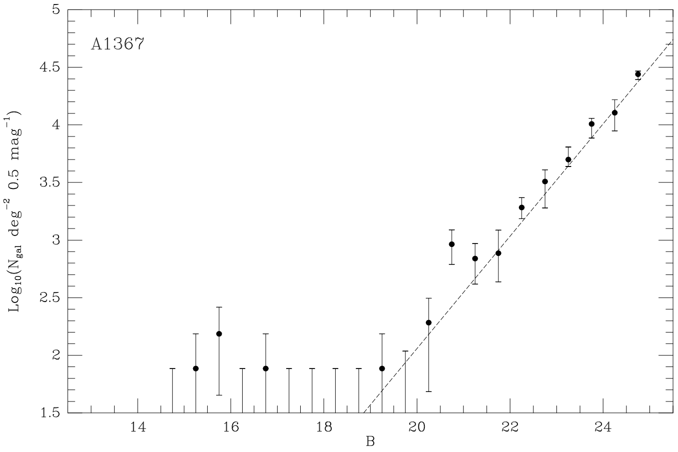
A1367
$\mathrm{Log}_{10}(N_{gal}\ \mathrm{deg}^{-2}\ 0.5\ \mathrm{mag}^{-1})$
1.5
2
2.5
3
3.5
4
4.5
5
14
16
18
20
22
24
B

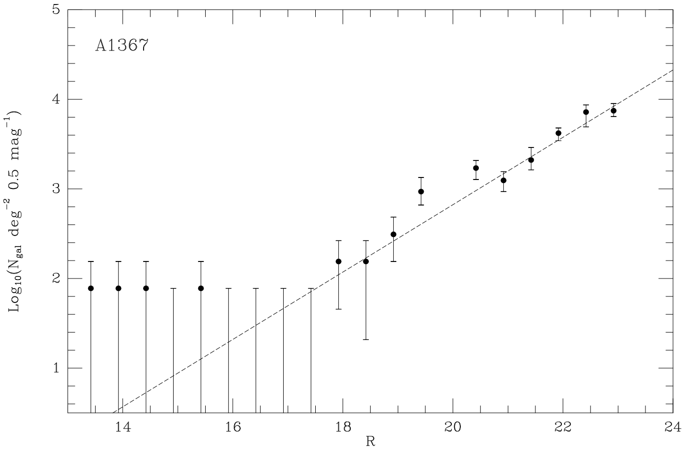
A1367
$\mathrm{Log}_{10}(N_{gal}\ \mathrm{deg}^{-2}\ 0.5\ \mathrm{mag}^{-1})$
1
2
3
4
5
14
16
18
20
22
24
R

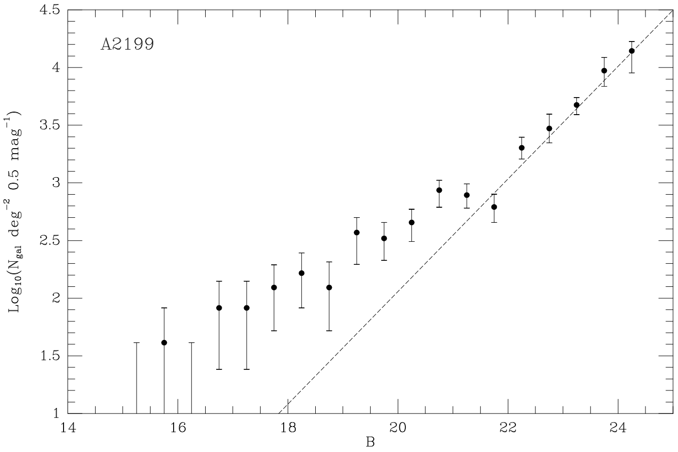
A2199
$\mathrm{Log}_{10}(N_{gal}\ \mathrm{deg}^{-2}\ 0.5\ \mathrm{mag}^{-1})$
1
1.5
2
2.5
3
3.5
4
4.5
14
16
18
20
22
24
B

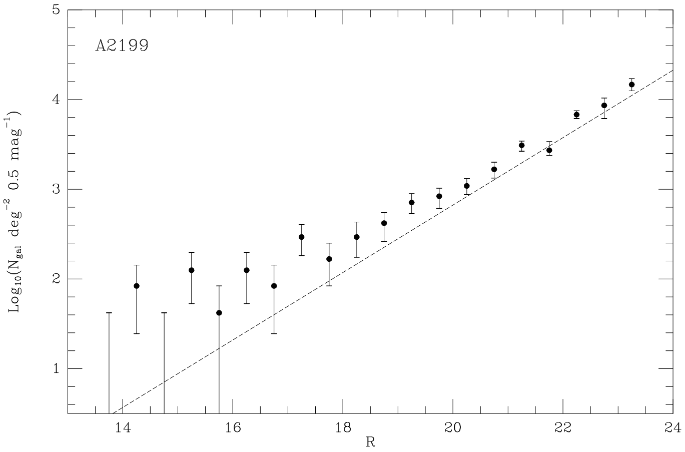
A2199
$\mathrm{Log}_{10}(N_{gal}\ \mathrm{deg}^{-2}\ 0.5\ \mathrm{mag}^{-1})$
1
2
3
4
5
14
16
18
20
22
24
R

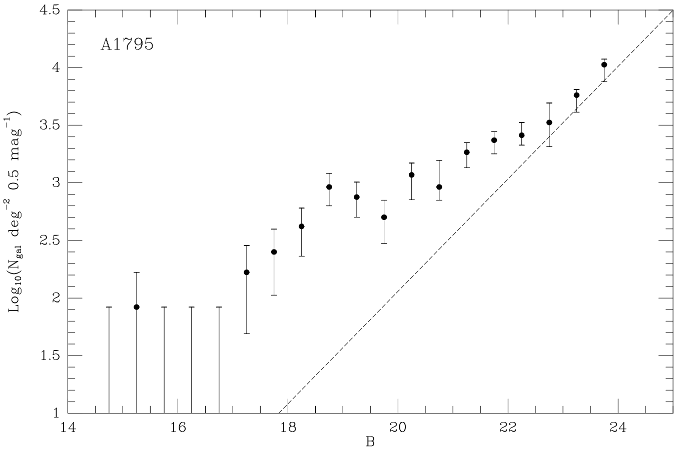
A1795
$\mathrm{Log}_{10}(N_{gal}\ \mathrm{deg}^{-2}\ 0.5\ \mathrm{mag}^{-1})$
1
1.5
2
2.5
3
3.5
4
4.5
14
16
18
20
22
24
B

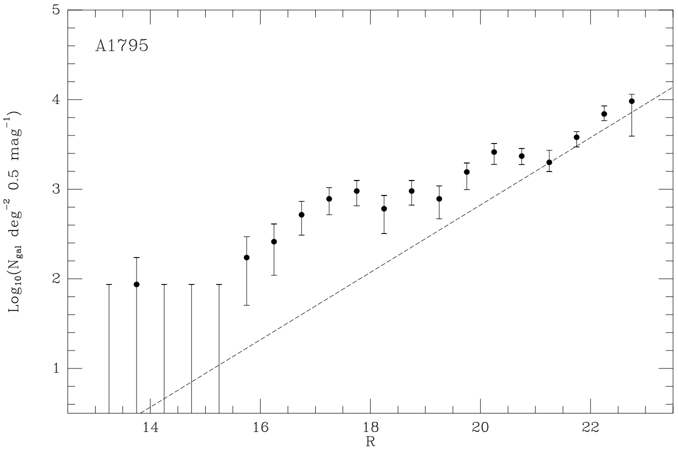
A1795
$\mathrm{Log}_{10}(N_{gal}\ \mathrm{deg}^{-2}\ 0.5\ \mathrm{mag}^{-1})$
1
2
3
4
5
14
16
18
20
22
R

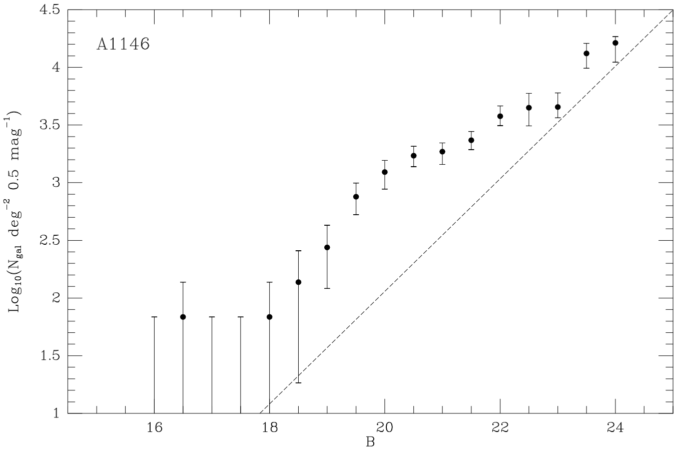
A1146
$\mathrm{Log}_{10}(N_{gal}\ \mathrm{deg}^{-2}\ 0.5\ \mathrm{mag}^{-1})$
1
1.5
2
2.5
3
3.5
4
4.5
16
18
20
22
24
B

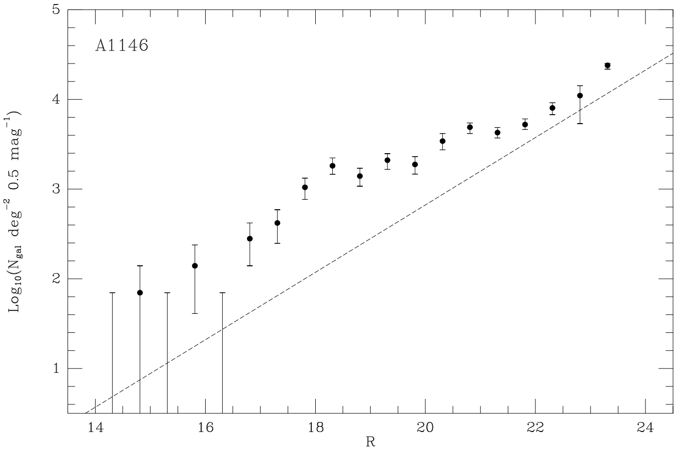
A1146
$\mathrm{Log}_{10}(N_{gal}\ \mathrm{deg}^{-2}\ 0.5\ \mathrm{mag}^{-1})$
1
2
3
4
5
14
16
18
20
22
24
R

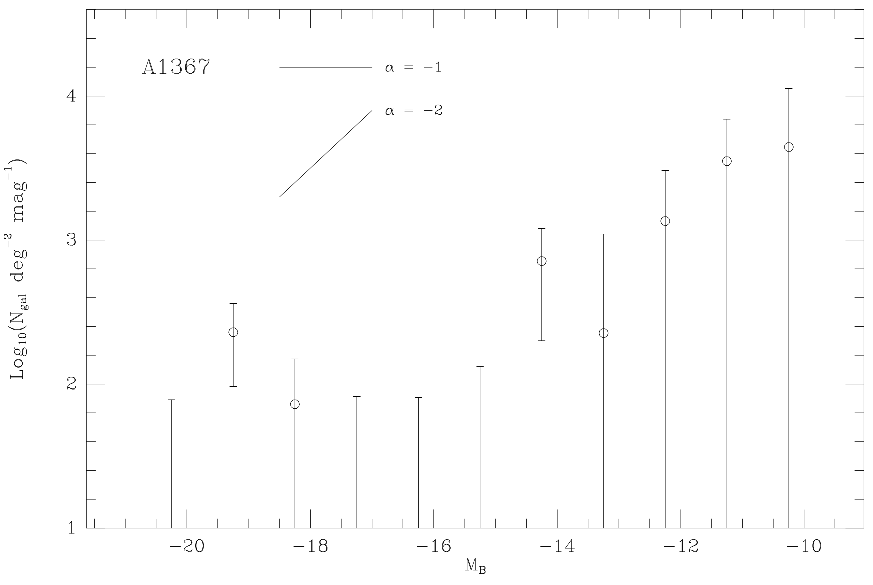
A1367
α = −1
α = −2
Log₁₀(N_gal deg⁻² mag⁻¹)
1
2
3
4
−20
−18
−16
−14
−12
−10
M_B

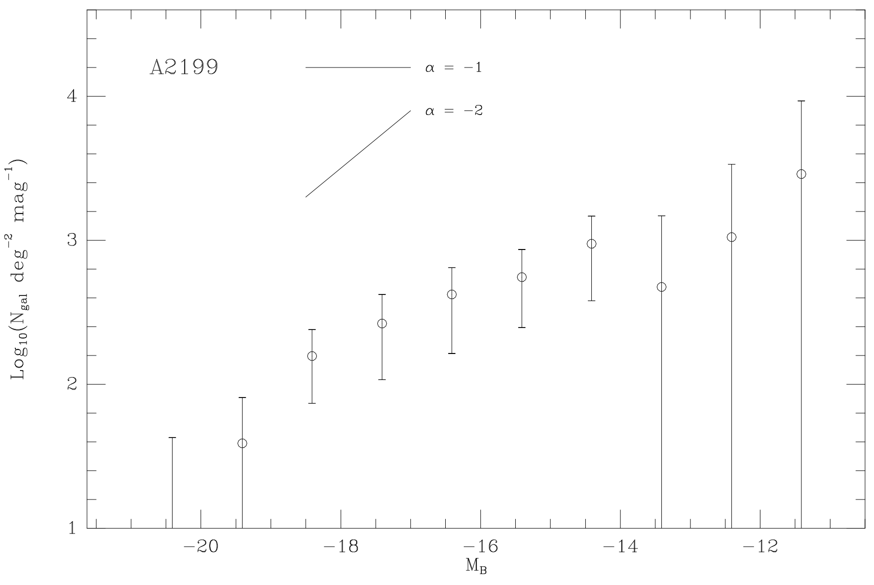
A2199
α = −1
α = −2
Log₁₀(N_gal deg⁻² mag⁻¹)
1
2
3
4
−20
−18
−16
−14
−12
M_B

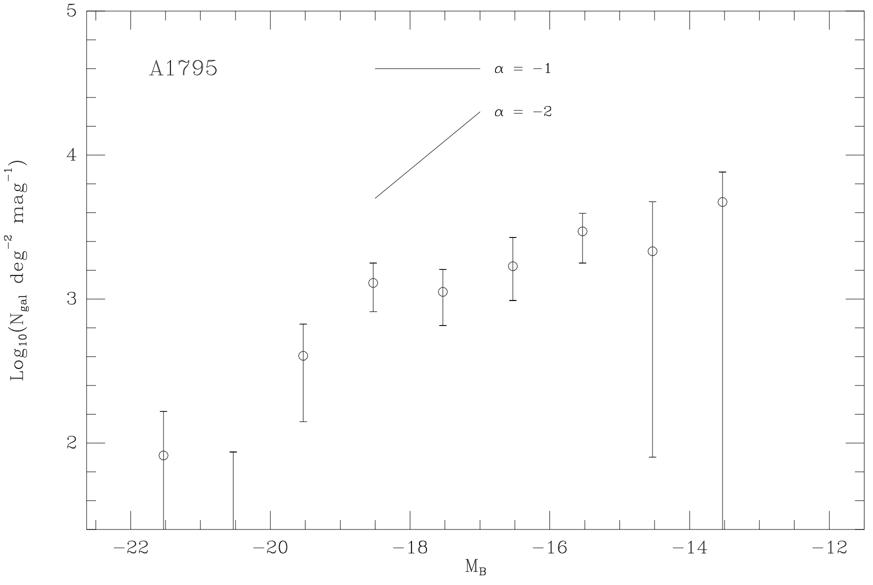
A1795
α = −1
α = −2
Log₁₀(N_gal deg⁻² mag⁻¹)
2
3
4
5
−22
−20
−18
−16
−14
−12
M_B

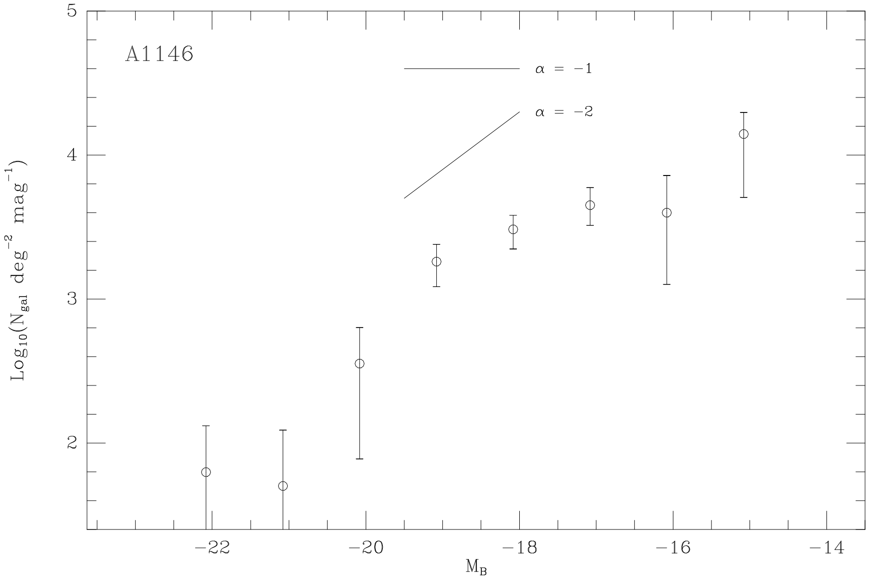
A1146
α = −1
α = −2
Log₁₀(N_gal deg⁻² mag⁻¹)
2
3
4
5
−22
−20
−18
−16
−14
M_B

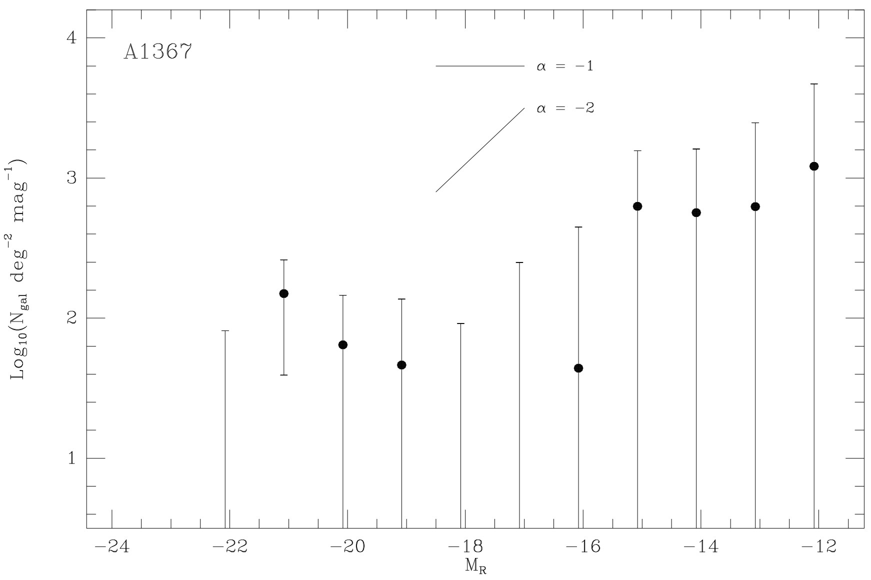
A1367
α = −1
α = −2
Log$_{10}$(N$_{gal}$ deg^{-2} mag^{-1})
1
2
3
4
−24
−22
−20
−18
−16
−14
−12
M$_R$

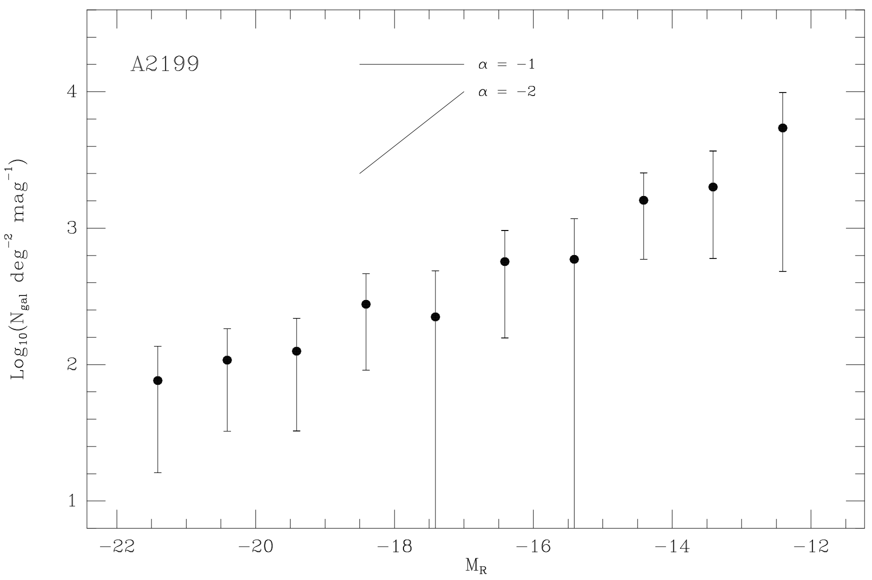
A2199
α = −1
α = −2
Log$_{10}$(N$_{gal}$ deg^{-2} mag^{-1})
1
2
3
4
−22
−20
−18
−16
−14
−12
M$_R$

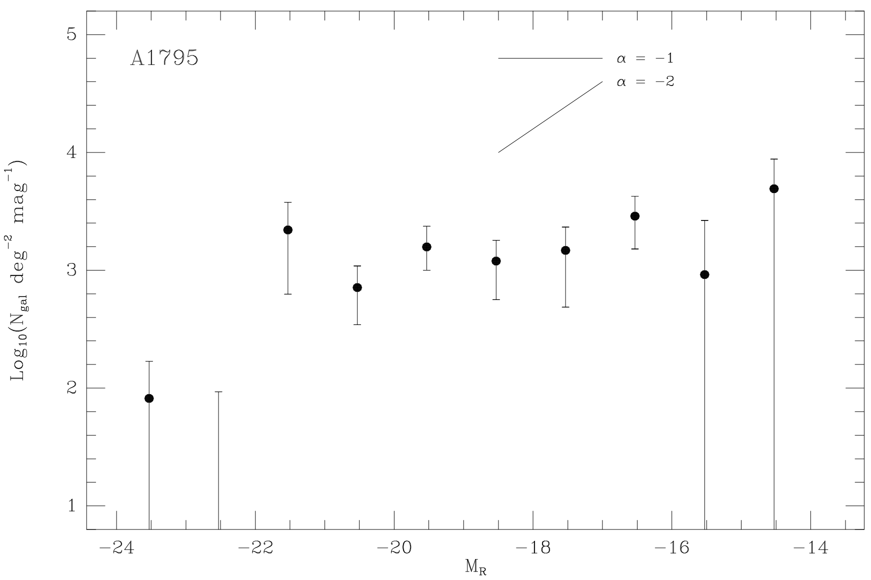
A1795
α = −1
α = −2
Log$_{10}$(N$_{gal}$ deg^{-2} mag^{-1})
1
2
3
4
5
−24
−22
−20
−18
−16
−14
M$_R$

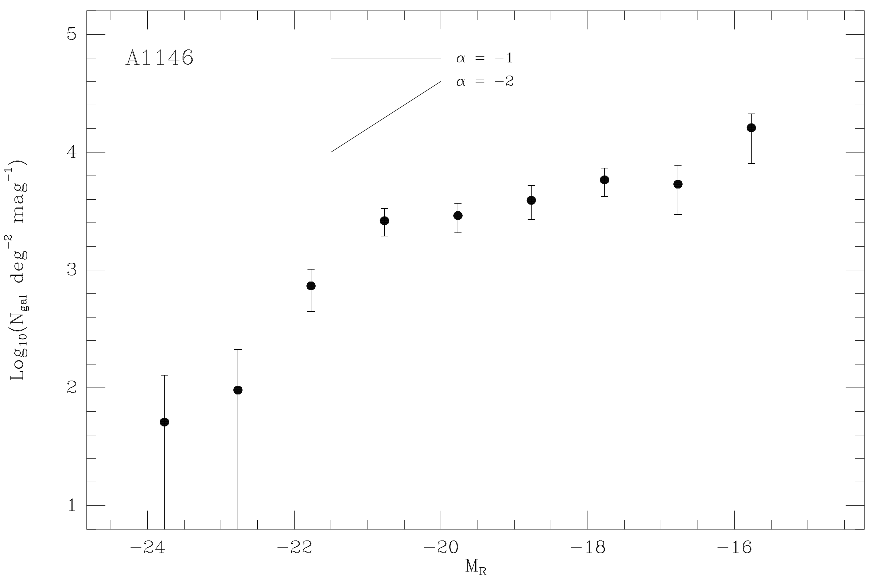
A1146
α = −1
α = −2
Log$_{10}$(N$_{gal}$ deg^{-2} mag^{-1})
1
2
3
4
5
−24
−22
−20
−18
−16
M$_R$

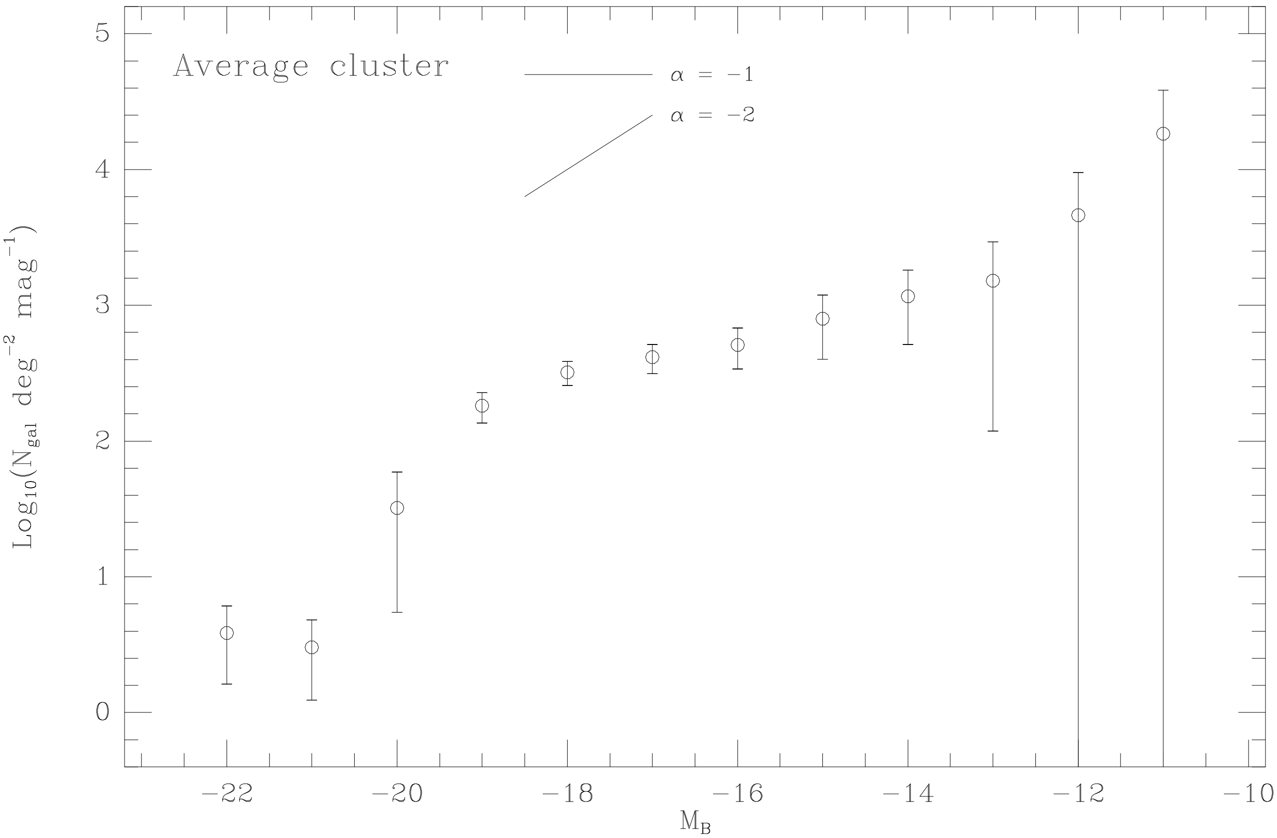
Average cluster
α = −1
α = −2
Log10(N_gal deg^−2 mag^−1)
M_B
−22
−20
−18
−16
−14
−12
−10
0
1
2
3
4
5

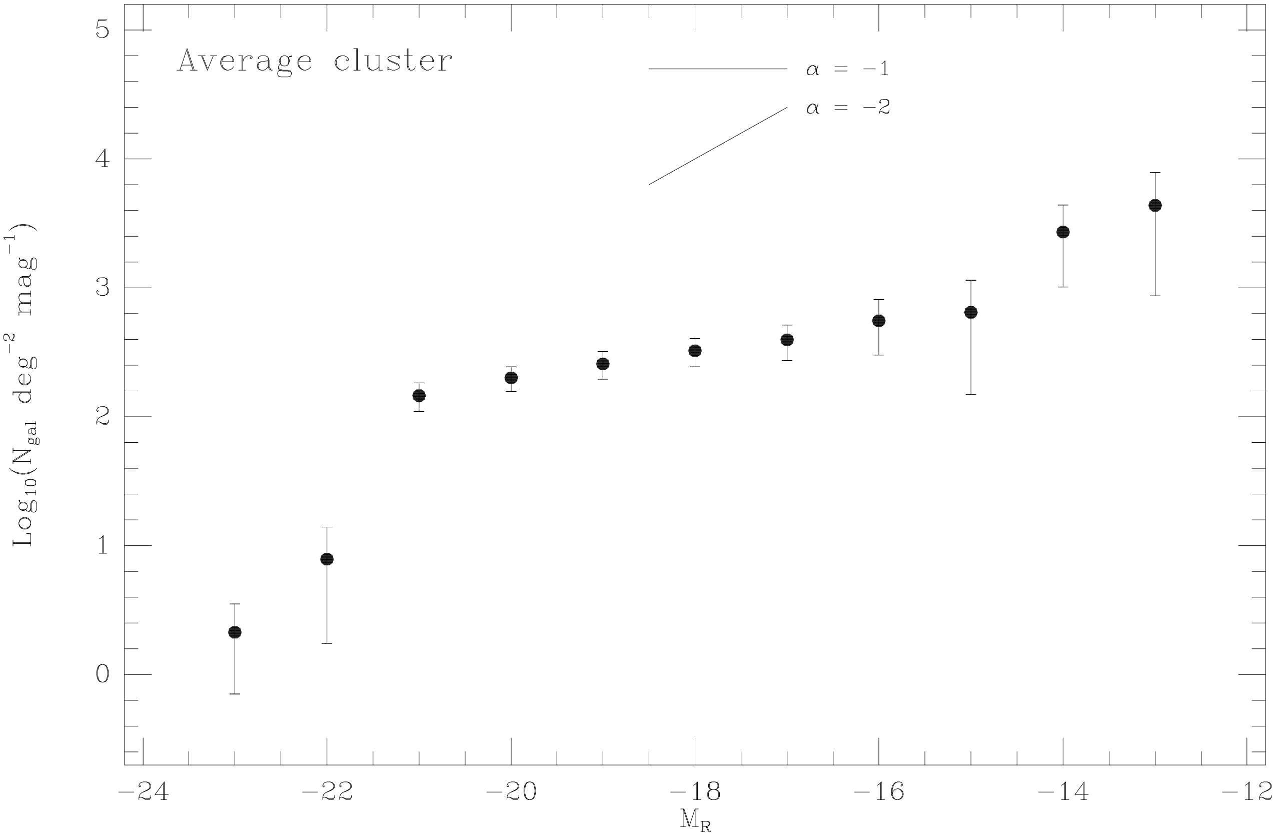
Average cluster
α = −1
α = −2
Log10(N_gal deg^−2 mag^−1)
M_R
−24
−22
−20
−18
−16
−14
−12
0
1
2
3
4
5

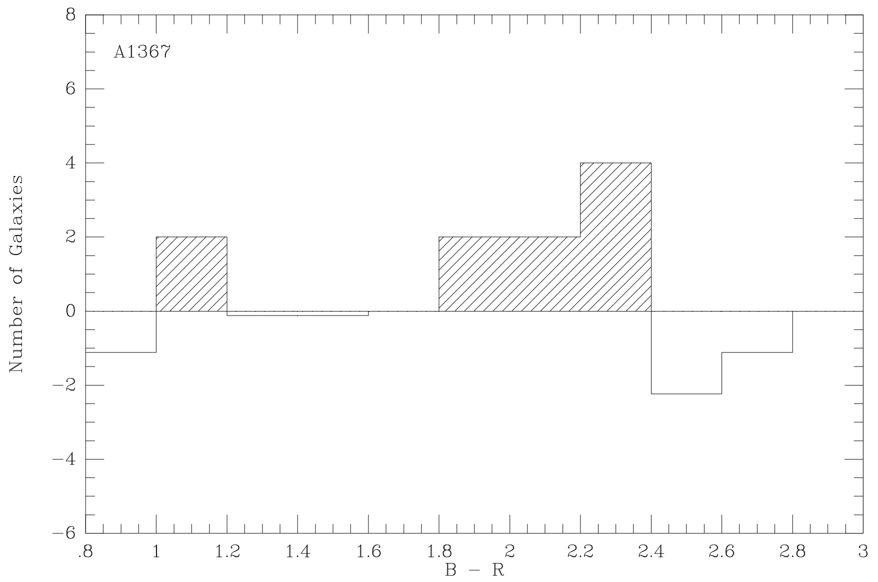
A1367
Number of Galaxies
B − R
8
6
4
2
0
−2
−4
−6
.8
1
1.2
1.4
1.6
1.8
2
2.2
2.4
2.6
2.8
3

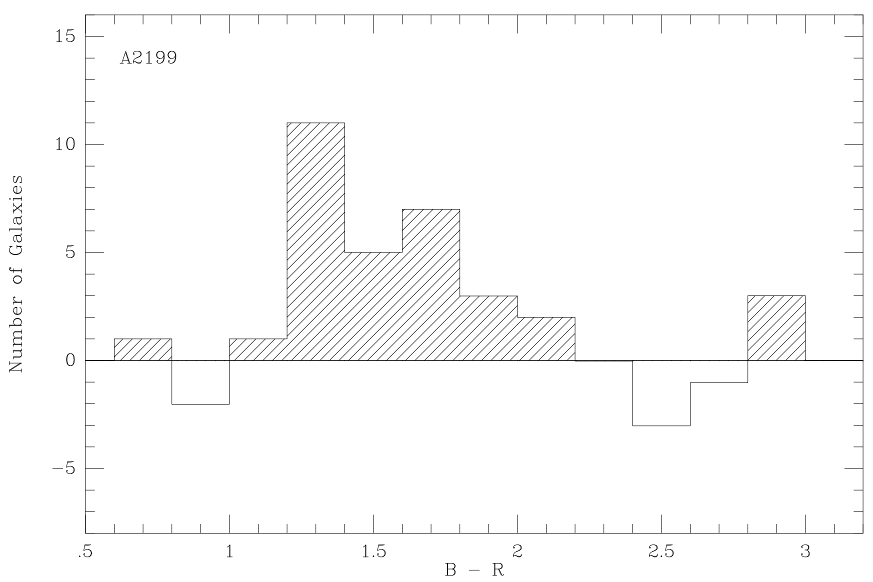
A2199
Number of Galaxies
B − R
15
10
5
0
−5
.5
1
1.5
2
2.5
3

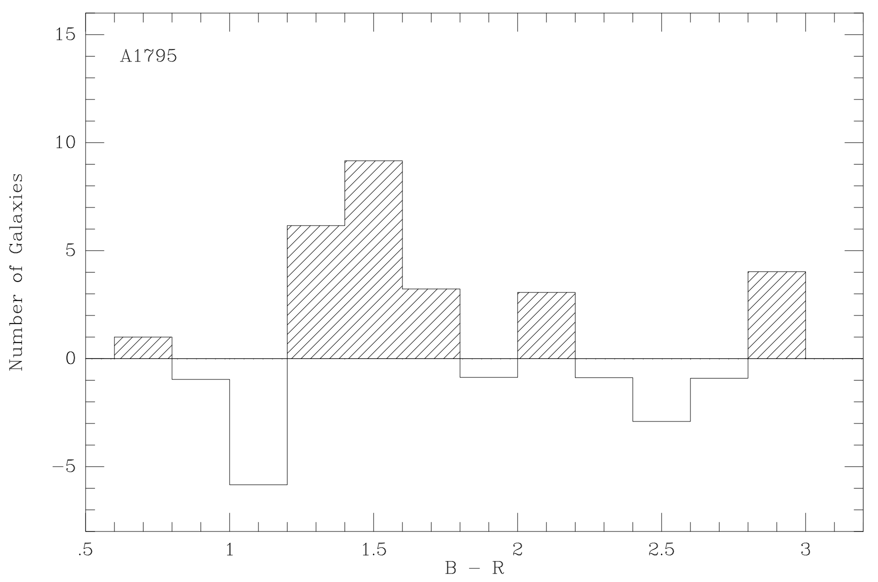
A1795
Number of Galaxies
B − R
15
10
5
0
−5
.5
1
1.5
2
2.5
3

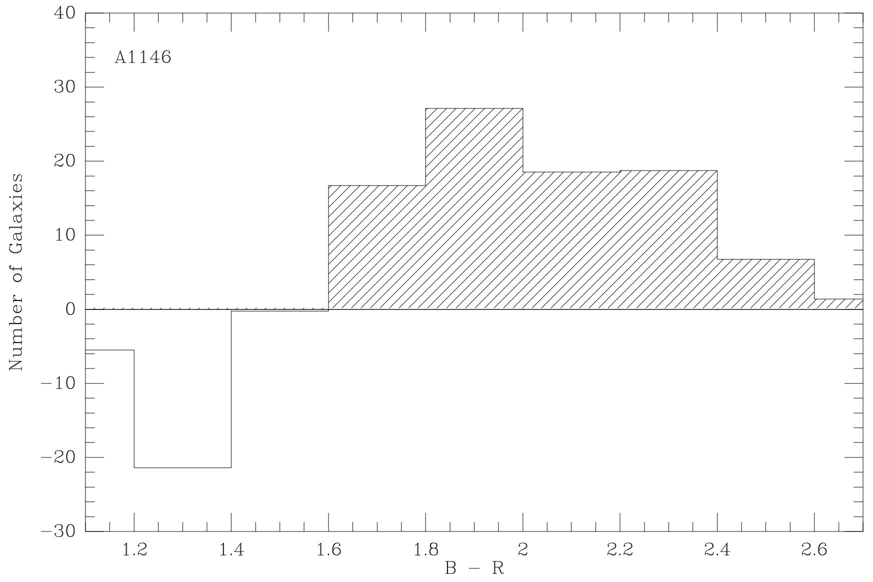
A1146
Number of Galaxies
B − R
40
30
20
10
0
−10
−20
−30
1.2
1.4
1.6
1.8
2
2.2
2.4
2.6

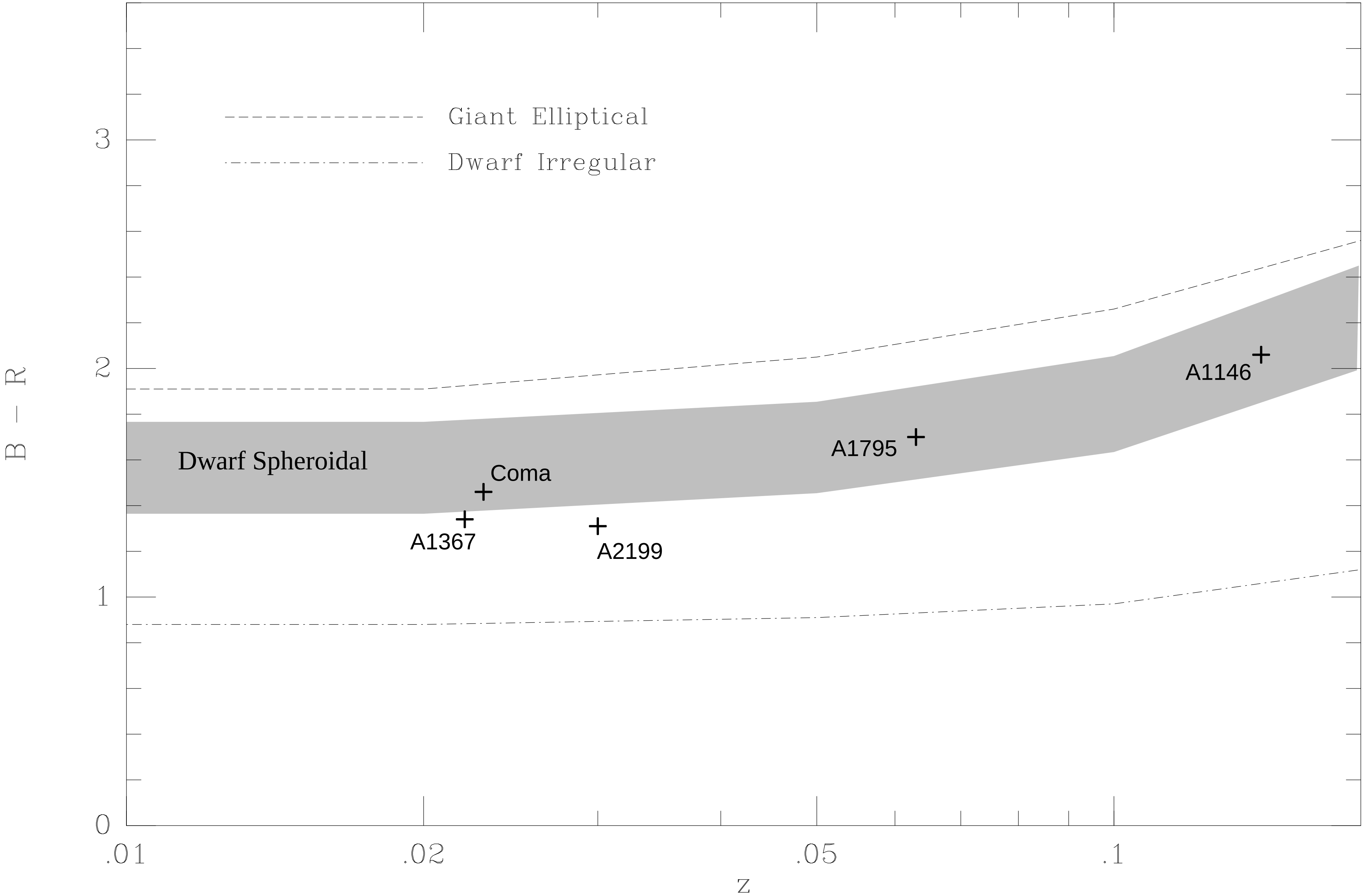
Giant Elliptical
Dwarf Irregular
Dwarf Spheroidal
Coma
A1367
A2199
A1795
A1146
B − R
0
1
2
3
.01
.02
.05
.1
z

Table 1

Properties of the Sample Clusters

Cluster	Richness (1)	z	σ km s^{-1}	L_x erg s^{-1}	A_B (2) mag	Σ_c g cm^{-2}	$\dot{M}$ M$_\odot$ yr $^{-1}$
A1367	2	0.022	822 (3)	2×10^{43} (4)*	0.00	4.1	0 (5)
A2199	2	0.030	860 (6)	9×10^{43} (4)*	0.00	3.1	150 (5)
A1795	2	0.063	887 (6)	2.3×10^{44} (4)*	0.00	1.6	478 (5)
A1146	4	0.141	1166 (3)	1.5×10^{44} (7)†	0.25	0.83	–

Assumes $H_0 = 75$ km s^{-1} Mpc^{-1}

* $0.5 - 3.0$ keV Luminosity

† $0.3 - 3.5$ keV Luminosity

References: (1) Abell 1958; (2) Burstein & Heiles 1982; (3) Zabludoff et al. 1990; (4) Jones & Forman 1984; (5) Fabian 1994; (6) Girardi et al. 1996; (7) Gioia & Luppino 1994

Table 2

Observing Log

Field	Color	Run*	Size (sq. arcmin)	α (1950)	δ (1950)	Exposure min	$< X >$ mag	FWHM arcsec
A1367	B	2	47.2	$11^{\mathrm{h}}41.9^{\mathrm{m}}$	$20°7.0'$	50	0.00	0.74
	R	2				45	0.40	1.03
A2199 I	B	2	41.1	$16^{\mathrm{h}}26.6^{\mathrm{m}}$	$39°34.8'$	35	0.00	0.97
	R	1				40	0.00	0.78
A2199 II	B	2	51.1	$16^{\mathrm{h}}26.6^{\mathrm{m}}$	$39°41.3'$	70	0.00	0.99
	R	2				50	0.00	0.92
A1795	B	3,4	44.7	$13^{\mathrm{h}}46.7^{\mathrm{m}}$	$26°50.0'$	66	0.15	1.32
	R	3,4				72	0.50	1.25
A1146	B	3	54.3	$10^{\mathrm{h}}58.8^{\mathrm{m}}$	$-22°27.7'$	60	0.13	1.10
	R	3				96	0.11	0.98

***Observing runs:** **1.** April 8–10 1994; **2.** May 7–8 1994; **3.** April 30 – May 3 1995; **4.** August 1 1995 (all UH 2.2 m with Tektronix 2048 × 2048 CCD at f/10)

Table 3

Composite B band luminosity function

M_B	$\log_{10} N$ (gal deg^{-2} mag^{-1})	α_{12}	α_{33}
-22.0	$0.586^{+0.198}_{-0.376}$	–	–
-21.0	$0.482^{+0.202}_{-0.389}$	–	–
-20.0	$1.508^{+0.262}_{-0.768}$	-2.41	–
-19.0	$2.260^{+0.097}_{-0.126}$	-2.32	-2.53
-18.0	$2.507^{+0.080}_{-0.098}$	-1.69	-1.48
-17.0	$2.617^{+0.095}_{-0.121}$	-1.37	-1.36
-16.0	$2.709^{+0.125}_{-0.177}$	-1.35	-1.33
-15.0	$2.400^{+0.175}_{-0.298}$	-1.37	-1.33
-14.0	$3.067^{+0.192}_{-0.354}$	-1.55	-1.44
-13.0	$3.182^{+0.284}_{-1.108}$	-1.83	–
-12.0	$3.663^{+0.313}_{-3.663}$	–	–
-11.0	$4.263^{+0.321}_{-4.263}$	–	–

Table 4

Composite R band luminosity function

M_R	$\log_{10} N$ (gal deg^{-2} mag^{-1})	α_{12}	α_{33}
-23.0	$0.328^{+0.222}_{-0.477}$	–	–
-22.0	$0.895^{+0.250}_{-0.650}$	–	–
-21.0	$2.165^{+0.098}_{-0.126}$	-2.39	–
-20.0	$2.304^{+0.084}_{-0.105}$	-1.87	-1.72
-19.0	$2.412^{+0.093}_{-0.119}$	-1.27	-1.00
-18.0	$2.511^{+0.096}_{-0.123}$	-1.27	-1.26
-17.0	$2.596^{+0.116}_{-0.159}$	-1.26	-1.15
-16.0	$2.744^{+0.164}_{-0.266}$	-1.51	-1.47
-15.0	$2.810^{+0.248}_{-0.639}$	-1.69	–
-14.0	$3.432^{+0.211}_{-0.426}$	–	–
-13.0	$3.640^{+0.256}_{-0.701}$	–	–